Photodiagnosis and Photodynamic Therapy 25 (2019) 66–73

Contents lists available at ScienceDirect

Photodiagnosis and Photodynamic Therapy

journal homepage: www.elsevier.com/locate/pdpdt

Real-time mapping of heat generation and distribution in a laser irradiated agar phantom loaded with gold nanoparticles using MR temperature imaging

Ali Farashahi[a,1], Arash Zare-Sadeghi[b,c,d,1], Ali Shakeri-Zadeh[c,d], S. Kamran Kamrava[c], Shayan Maleki[c], Habib Ghaznavi[e,*], Fariborz Faeghi[a,*]

[a] Radiology Department, School of Allied Medical Sciences, Students Research Committee, Shahid Beheshti University of Medical Science, Tehran, Iran
[b] Skull Base Research Center, The Five Senses Institute, Iran University of Medical Sciences (IUMS), Tehran, Iran
[c] ENT and Head & Neck Research Center and Department, The Five Senses Institute, Iran University of Medical Sciences (IUMS), Tehran, Iran
[d] Medical Physics Department, School of Medicine, Iran University of Medical Sciences (IUMS), Tehran, Iran
[e] Health Promotion Research Center, Zahedan University of Medical Sciences (ZaUMS), Zahedan, Iran

ARTICLE INFO

Keywords:
Gold nanoparticles
Laser
Photothermal therapy
Thermal distribution
MRI
Imaging

ABSTRACT

Gold nanoparticles (AuNPs) have shown potential strength in photothermal therapy of cancer. Several techniques have been developed to investigate local heat generation by AuNPs. However, a sensitive thermal imaging technology with high temporal resolution, minimum invasiveness and high spatial resolution is still lacking. In this research study, by using magnetic resonance thermal imaging (MRTI), we reported a technique for monitoring of heat generation and distribution in an AuNPs loaded agar phantom irradiated by laser.

Three different agar phantoms with various AuNPs concentrations (0, 8 and 16 μg/ml) were produced and studied. The phantoms were exposed to an external laser [532 nm; 4 min] under MRTI. For real-time temperature monitoring, we employed the theory of proton resonance frequency (PRF) shift. Infrared (IR) camera was employed to measure the actual temperature of each point on the surface of irradiated agar gel. Finally, the correlation between the temperatures obtained by IR camera and MRTI was evaluated.

We observed that temperature of the gels loaded by AuNPs at concentration of 0, 8 and 16 μg/ml reached 27.2, 37.8, 45 °C with a total area of heat distribution of 94.98, 452.16, and 907.34 mm^2 (from the point of irradiation). During the process of laser irradiation, we observed: (i) a significant rise in temperature, (ii) a dependency between the rate of temperature rise and concentration of AuNPs, and (iii) a direct correlation between temperature change and MR image phase. In addition, statistical analysis showed that the variation of temperatures measured by IR camera and temperatures computed by MRTI had acceptable correlation ($R > 0.9$).

In conclusion, MRTI has a good sensitivity and precision that can be employed for nano-photothermal therapy planning and may be considered for real-time mapping of heat generation and distribution in a laser irradiated tissue loaded by AuNPs.

1. Introduction

Photothermal therapy (PTT) is a successful technique recently employed for the treatment of malignant tumors [1–4]. It is important for the introduction of light-absorbing materials into the tumor to increase the effectiveness of photothermal effects and consequently to enhance the selectivity of PTT method [5]. An increasing number of optically activated metal-based nanoparticles are being investigated in the area of PTT technique. These nanoparticles have an interesting property such that their conduction band electrons exhibit a plasmon resonance. Such property of these nanoparticles significantly increases the cross section of laser absorption if the frequency of the incident laser is close to the resonance frequency of the nanoparticles [6,7]. Accordingly, gold nanoparticles (AuNPs) became suitable useful agents for PTT on account of their enhanced laser absorption cross section such that they ensure efficacious laser therapy at relatively lower energies and

* Corresponding authors.
E-mail addresses: dr.ghaznavi@zaums.ac.ir (H. Ghaznavi), f_faeghi@sbmu.ac.ir (F. Faeghi).
[1] These authors contributed equally to this work.

https://doi.org/10.1016/j.pdpdt.2018.11.010
Received 12 August 2018; Received in revised form 29 September 2018; Accepted 13 November 2018
Available online 14 November 2018
1572-1000/

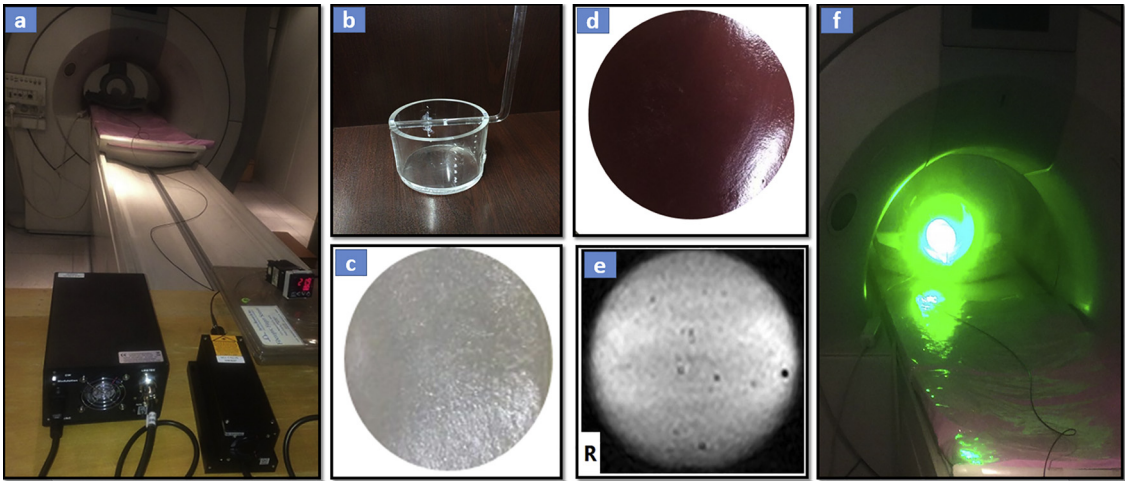

Fig. 1. (a) experimental setup, (b) prepared container/phantom, (c) a section of agar phantom, (d) a section of agar phantom containing AuNPs, (e) MR image of agar phantom, (f) an image of experimental set-up while phantom was irradiated by laser in MRI gantry.

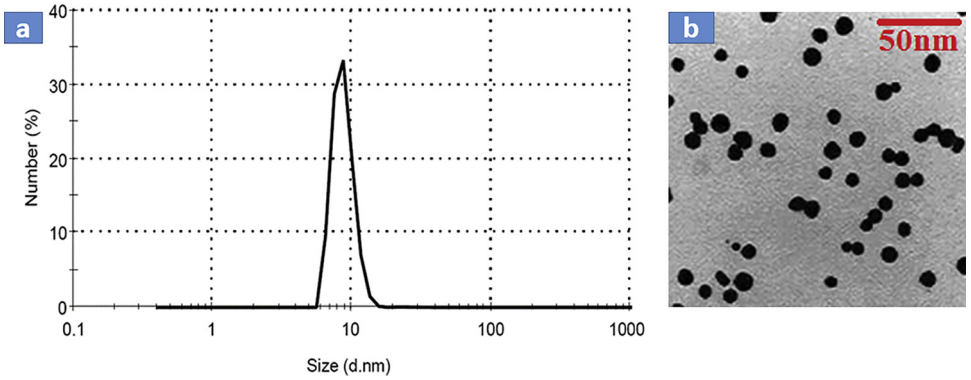

Fig. 2. TEM and DLS of the prepared AuNPs. (a) The size distribution of the AuNPs shows the main frequency of nanoparticles is ~ 10 nm. (b) TEM image of AuNPs shows that the nanoparticles are spherical in shape with the size ranged.from 5 to 15 nm.

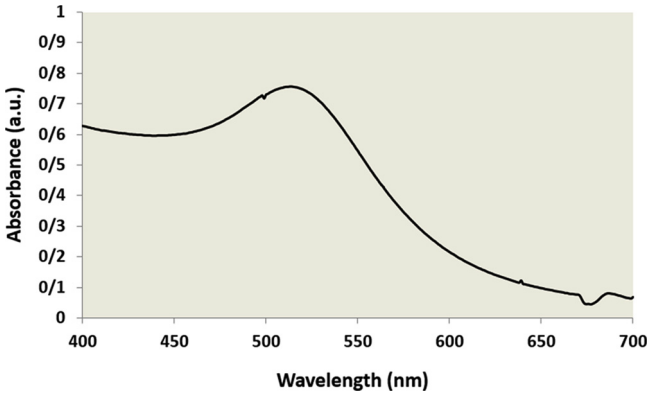

Fig. 3. The absorption spectrum of AuNPs utilized for making nanoparticles loaded agar phantoms.

consequently render the PTT technique minimally invasive [8–12].

In order to increase the therapeutic efficiency of PTT in the clinics, real-time mapping of temperature as well as estimation of thermal dose are quite necessary and may provide us with appropriate and effective strategy [13]. Unfortunately, it is too difficult to measure the actual temperature of the tissue when irradiated by laser. Physiological processes may alter local heat generation and distribution. On the other hand, blood flow may increase during rise in temperature and thus change heat conduction of a tumor and its collateral tissues. Consequently, real-time mapping of temperature is essential, and imaging modalities may be one of the best choices for which MRI seems to be an ideal tool for temperature mapping [6]. MR thermal imaging (MRTI), which is non-invasive and volumetric in its nature, as opposed to thermistors or thermocouples which are invasive and only provide point measurements, might well be used for volumetric thermometry [14]. Unfortunately, temperature imaging tools are not routinely available on clinical MRI instruments and this defect might limit its use in clinical research and practice.

To set MRTI, three main parameters have been fully investigated with respect to their temperature dependence; the spin–lattice relaxation time ($T1$), the molecular diffusion coefficient and the proton resonance frequency (PRF). Among the various MRI techniques, the PRF shift method has been shown to be the most accurate [15]. The local magnetic field (magnetic flux density), B_{loc} experienced by a proton within an object is related to the main magnetic field of the MRI scanner, B_0, according to:

$$B_{loc=}(1-\sigma_{tot})B_0 + \delta B_0 \quad (1)$$

Where σ_{tot} the total screening constant of the proton and δB0 is represents the local deviations from B_0 that are not temperature dependent. When the temperature increases, the total screening constant increases (linearly) inducing a decrease in B_{loc}. Subtraction of two phase images of the same volume (slice) obtained at different times will reveal temperature changes between image acquisitions. According to the Larmor equation, the phase (in radians) measured within a voxel at a temperature T is given by:

$$\varphi(\mathrm{T}) = \gamma T_E[(1-\sigma_{tot}(T))B_0 + \delta B_0] \quad (2)$$

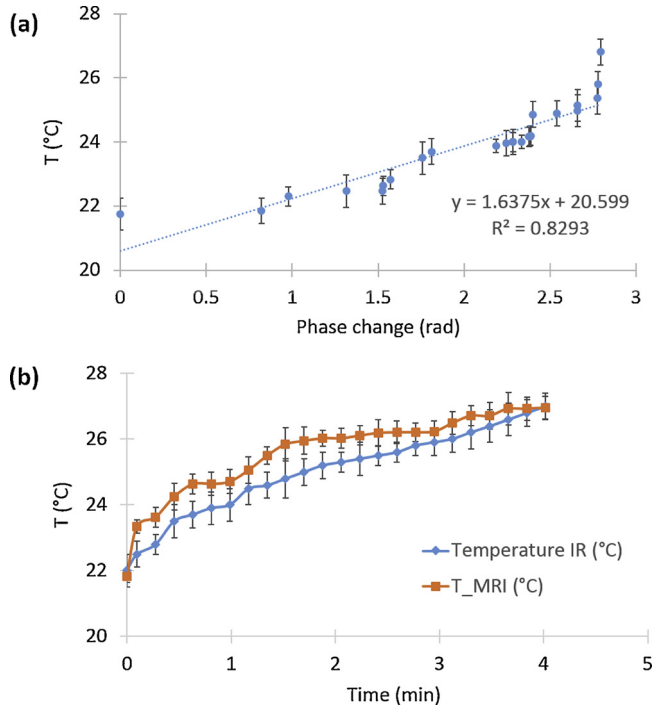

Fig. 4. The plot of (a) temperature changes against phase changes for a laser irradiated agar gel (C_{AuNPs} = 0) and (b) temperature changes measured by IR camera and calculated by MRTI against laser irradiation time (Correlation coefficient R = 0.952).

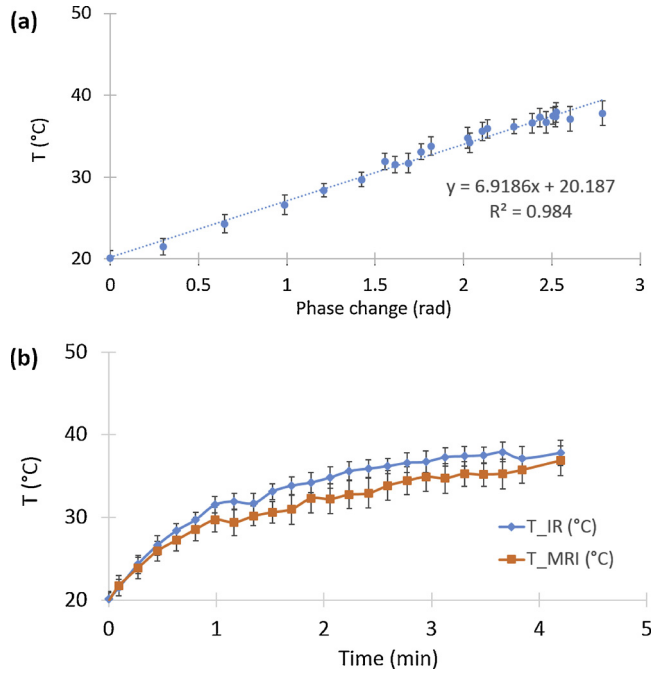

Fig. 5. The plot of (a) temperature changes against phase changes for a laser irradiated agar gel (C_{AuNPs} = 8 μg/ml) and (b) temperature changes measured by IR camera and calculated by MRTI against laser irradiation time (Correlation coefficient R = 0.991).

Where γ is the gyromagnetic ratio of hydrogen ($\gamma/2\pi = 42.577 \times 10^6$ s^{-1} T^{-1}) and *TE* is the echo time of the pulse sequence. If a second image is obtained when the temperature within the same voxel has changed to T', a different phase would be measured. Subtraction of the first image from the second image results in a phase difference within the voxel according to [15]:

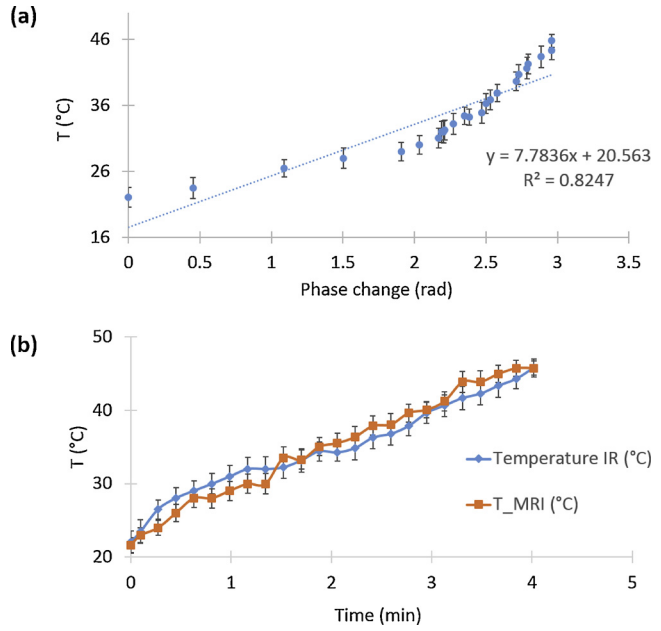

Fig. 6. The plot of (a) temperature changes against phase changes for a laser irradiated agar gel (C_{AuNPs} = 16 μg/ml) and (b) temperature changes measured by IR camera and calculated by MRTI against laser irradiation time (Correlation coefficient R = 0.992).

$$\Delta\varphi = \varphi(T') - \varphi(T) = \gamma T_E[\sigma_{tot}(T) - \sigma_{tot}(T')]B_0 = -\gamma T_E \alpha \Delta T B_0 \quad (3)$$

Where α is the proportionality constant in the linear temperature dependence of σ_{tot} [16].

As stated before, several techniques have been developed to investigate local heat generation by AuNPs in the process of laser hyperthermia [17–22]; however, a sensitive thermal imaging technology with high temporal resolution, minimum invasiveness and high spatial resolution is still lacking. In this research study, based on the PRF theory described above, we reported a non-invasive technique for real-time mapping of heat generation and distribution in a laser irradiated agar phantom loaded by AuNPs employing MRTI.

2. Materials and methods

2.1. Materials

The gold nanoparticle (NB-AuNP-20 nm) was purchased from Nanobon Company (Tehran, Iran). Agar powder was purchased from Sigma Chemical Co. (USA). A customized phantom made of Plexiglas was used for MR imaging (Fig. 1). The Plexiglas phantom was cylindrical in shape (diameter: 100 mm; height: 100 mm). Ten holes at different distances (intervals: 10 mm) were placed on the phantom wall for insertion of thermocouple probe into the agar phantom.

2.2. Nanoparticles characterizations

The absorption peak of the purchased AuNPs was determined using spectrophotometer (Ray leight UV-1601). For this purpose, a sample was diluted in distilled water and its absorption spectrum in the range of visible wavelengths (400–700 nm) was measured.

The mean diameter of the nanoparticles was measured employing dynamic light scattering (DLS) instrument (NanoZS, Malvern, UK). Nanoparticles were homogenized in distilled water and irradiated by ultrasound for 10 min; then, the sample was transferred into a cuvette and the required measurements were made.

Shape and size of the prepared AuNPs were also investigated by transmission electron microscope (TEM, Zeiss, LEO 906). In this section

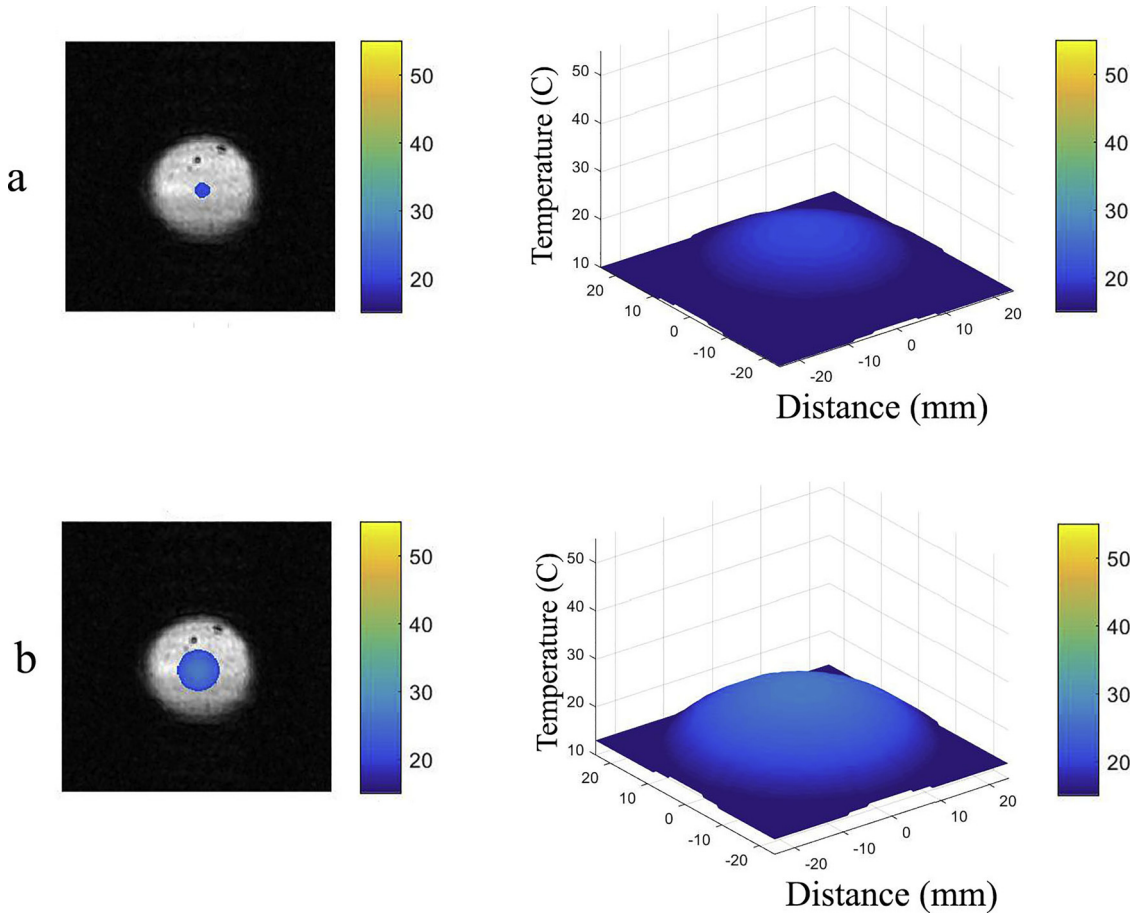

Fig. 7. Thermal dirstibution in agar gel phantom (C_{AuNPs} = 0). Two and three dimensional color map images of agar gel (a) before and (b) after laser irradiation.

of the study, AuNPs was immersed in 2 ml distilled water and treated with ultrasound for 10 min. Then, 10 µl of the solution was carefully dropped into copper grid and dried. Finally, TEM observation was made and photographs were obtained.

2.3. Preparation of agar phantom

After characterization of AuNPs, three phantoms containing 2% agar powder were prepared. The first phantom was only made of agar gel (without any AuNPs), the second agar phantom had 8 µg/ml AuNPs, and the third phantom had 16 µg/ml AuNPs. To prepare the gel, 2 g agar powder was added to 100 ml distilled water. The mixture was heated in a microwave oven (500 W), and occasionally stirred until it started boiling. Boiling was then allowed for about 1 min and the evaporated water was replaced. Afterwards, the liquid agar gel was poured into Plexiglas cylinder and allowed to cool at room temperature. Fig. 1 shows some photos of the experimental set-up as well as MR image of agar phantom.

2.4. Laser irradiation

An optical fiber having a length of 4 m and a power transmission of 80% to 90% was inserted into the applicator to deliver the photons from a laser device (λ = 532 nm; Power = 2.24 W; Changchun New Industries Optoelectronics Tech; China) to the agar phantom.

2.5. MR imaging

All images were taken by a 1.5 T MRI scanner (Gyroscan, Philips). Magnetic resonance temperature imaging (MRTI) was performed using a 2D fast GRE-EPI sequence for phase-sensitive imaging. The following parameters were employed:

Square field of view = 16 cm; slice thickness = 1.5 mm; acquisition matrix = 192 × 192; TR = 115 ms; TE = 25 ms; flip angle: 40°.

The body resonator was used for excitation and receive-only surface coil was employed for signal reception. The parameters were set such that a high image quality and signal to noise ratio (SNR) were achieved within a reasonable acquisition time (each image was obtained every 5.7 s). The images were processed using Matlab software.

2.6. Thermometry

Infrared (IR) camera (Testo 875i, Germany) was used to estimate the actual temperature of each point on the surface of irradiated agar gel. On the other hand, the PRF technique was used to compute the temperature from MRTI results. The first image in each series was employed as the reference image and the phase shift of subsequent images in relation to this image accounted for temperature change between images. However, it has been demonstrated that the phase shift does not have a linear correlation with the real temperature measured using other methods like IR camera. The difference between the thermal values gathered by IR camera and temperatures estimated using MRTI was compensated with alpha (in Eq. (3)). The preceding studies [6,23,24] employed a single alpha for all cases (different laser powers, radiation times, and nanoparticle concentrations). In our study, the value of alpha was computed by matching the estimated and real temperatures in the coolest and hottest points of each series. It must be noted the calculated alpha values were ranged from 0.97 (for the samples without nanoparticles) to 1.05 (for the samples with nanoparticles). Accordingly, to increase the accuracy and sensitivity of the

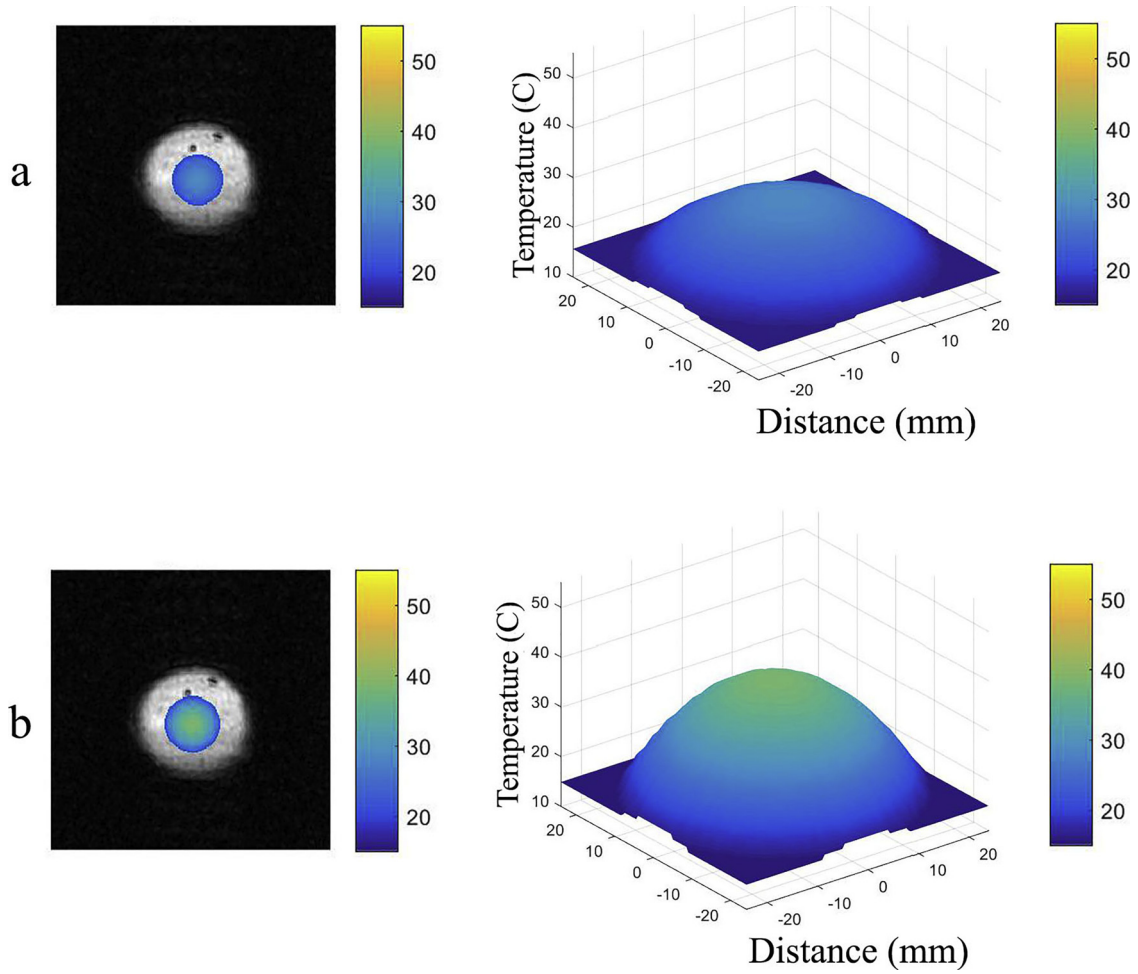

Fig. 8. Thermal dirstibution in AuNPs loaded agar gel phantom (C_{AuNPs} = 8 μg/ml). Two and three dimensional color map images of agar gel (a) before and (b) after laser irradiation.

measurements, we separately calculated alpha for each case.

2.7. Production of temperature map

The color map was generated using standard blue-yellow map with a temperature distribution of 15–45 °C (observed temperatures in our studies). The selected circular ROI (with radius of 25 mm) was centered on the laser irradiation point. The resulting colored maps were superimposed on the first image (obtained before laser irradiation) to demonstrate the distribution of heat around the irradiation point.

2.8. Statistical analysis

We compared the differences between the real temperature (obtained by IR camera) and the calculated temperature (from the MR images). Correlation analysis was employed to quantify the variation between the measured and calculated temperatures.

3. Results

The prepared AuNPs were investigated to determine their size and light absorption properties. Fig. 2 shows the results of DLS analysis and TEM of the prepared nanoparticles. As seen in Fig. 2, the nanoparticles had spherical shape and their size ranged from 5 to 15 nm. Fig. 3 shows the absorption spectrum of the nanoparticles, demonstrating that the absorption peak was at 520 nm. Accordingly, we selected a green laser to irradiate agar phantom.

After characterization of AuNPs, three phantoms containing various concentrations of AuNPs were produced as described in Section 2.3. Laser irradiation of the phantoms and MR imaging were done to measure:

i) the temperature changes (obtained by IR camera) versus time,
ii) the phase changes (obtained from MR images) versus time,
iii) the variations of temperature (obtained by IR camera) versus phase changes (obtained from MR images).

Figs. 4–6 shows the results obtained for various agar phantoms containing 0, 8 and 16 μg/ml AuNPs irradiated by laser. The changes of actual temperature (measured by IR camera) versus MR image phase is shown in Figs. 4–6(a), (a). During the process of laser irradiation, significant rise in temperature was observed. The center of agar gels irradiated by laser was measured to determine the variation in temperature. We observed that the center of gels loaded by 0, 8 and 16 μg/ml AuNPs experienced heating up to 27.2, 37.8, 45 °C. As seen in Figs. 4–6(a), there is a direct correlation between change of temperature and MR image phase. An increase in temperature resulted in a change in phase. To calculate the temperature of each point of the phantom employing MRTI, the phase change was first computed and then it was incorporated into the fitted line equation. We found that the temperature change measured by MRTI and IR camera had the same trend. Good correlation was found between data obtained by IR camera and temperature computed by PRF method. According to Figs. 4–6(b), it was also observed that the rate of temperature rise was dependent on

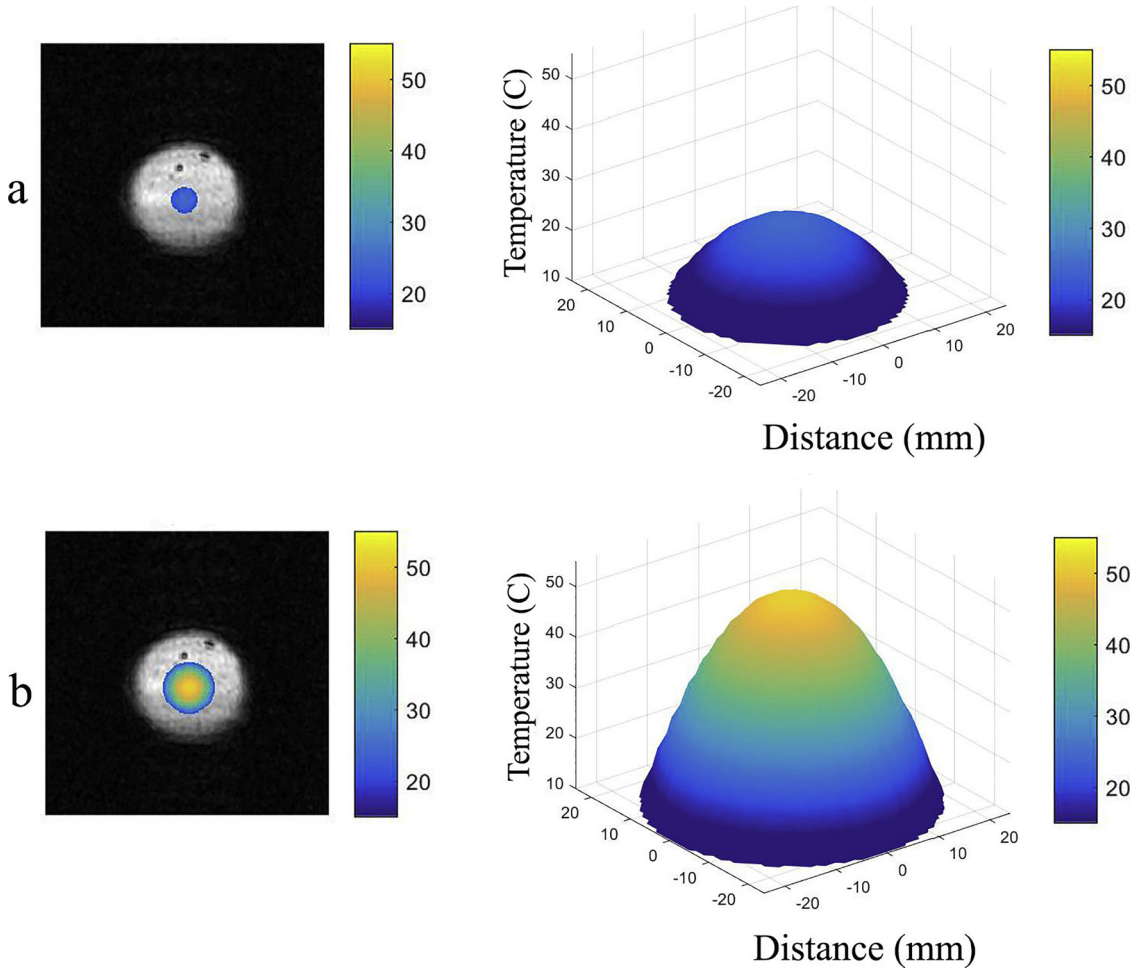

Fig. 9. Thermal dirstibution in AuNPs loaded agar gel phantom (C_{AuNPs} = 16 μg/ml). Two and three dimensional color map images of agar gel (a) before and (b) after laser irradiation.

the concentration of AuNPs.

Figs. 7–9 illustrate two and three dimensional color maps showing thermal distribution in the phantoms from the center (the location of laser irradiation) to different distances. As seen in superimposed images (Figs. 7–9), the highest temperature changes were observed on laser irradiation point (center of phantoms), and the points with further distance from the center had lower temperature changes. In addition, it was observed that temperature in certain radial points (e.g. 20 mm) in the phantom with the highest concentration of AuNPs (C_{AuNPs} = 16 μg/ml) was at higher level in comparison to the same points in other phantoms (C_{AuNPs} = 0 or 8 μg/ml). As seen in Figs. 7–9, the gels loaded by 0, 8 and 16 μg/ml AuNPs experienced various heating, and the total areas of heat distribution in these phantoms were up to 94.98, 452.16, and 907.34 mm^2 from the point of irradiation.

4. Discussion

In order to investigate the potential of the AuNPs as nanoheaters, suspensions of NPs in 2% agar at concentrations of 0 (control), 8 and 16 μg/ml were prepared. The phantom material should have thermal and optical properties similar to the soft tissues. Agar gel has often been employed for such purposes because it is fairly similar to soft tissues, such as muscle and liver, with a water content between 70% and 85% [25]. Agar gel is also used in studying thermal behavior of nanoparticles such as AuNPs in the presence of external sources of energy. For example, Curtis et al., recently investigated heat distribution of hybrid iron oxide-gold nanoparticles in an agar phantom [23].

Moreover, agar gel is widely used in MRI studies because it has approximately the same properties as water. It has been demonstrated that agar gel is suitable for the study of PRF technique in a wide temperature range and there is approximately a linear correlation between PRF shift and temperature change in agar gel [26].

The gels were formed in the prepared phantom (Fig. 1b). The agar gel samples (with and without AuNPs) at MRI room temperature were positioned in the direction of laser beam and were exposed to laser beam. Spherical AuNPs strongly absorbed laser energy because the coherent oscillations of the metal conduction band electrons were in strong resonance with visible frequencies of light [27]. This phenomenon is known as the surface plasmon resonance (SPR) [3,28], which strongly depends on size and shape of the nanoparticles [10,29]. The photothermal properties of AuNPs are due to photo-excitation of Au nanostructure, which result in the formation of a heated electron gas [30]. Such a hot gas subsequently cools quickly within ~1 ps through exchange of energy with its neighboring lattice and could be employed for the heating of the local environment [31], which is the basis of cancer photothermal therapy [7,32].

In order to increase the therapeutic efficiency of photothermal therapy in the clinics, real-time mapping of temperature and estimation of thermal dose are quite essential and may provide us with appropriate and efficacious strategy. Thermocouple is the simplest device, which may be used for real-time thermometry, but it is invasive and cannot offer 2-D information. This is while infrared camera is preferred. It provides real-time data as well as 2-D information. As stated before, Curtis et al., recently investigated heat distribution of hybrid iron oxide-

gold nanoparticles in an agar phantom employing thermocouple and IR camera [23]. They also compared the reliability of these measurement techniques. They demonstrated that thin wired thermocouple data possessed notably higher standard deviations than the infrared camera measurements. Infrared imaging permits increased data points and more sensitive and robust data compared to the thermocouple, but such imaging modality is able to provide thermal information from the surface of an object [23].

Overall, various technologies for thermometry reported to date fall into two categories: (i) scanning probe and (ii) non-scanning probe based strategies. The former includes scanning thermal microscopy [33], scanning photothermal microscopy [18], Raman thermometry [19] while the latter includes methods that employs nano-thermometers [20], fluorescent probes [34] and infrared cameras [21]. Each technology has its own unique strengths as well as distinct weaknesses. The most important advantage of MRTI over the mentioned thermometry techniques is its ability to provide an image of heat generation and distribution in a (biological) medium. Additionally, MRTI may map the rapid spatiotemporal distributions of heat distribution in soft tissues. In this study, as seen in part (b) of Figs. 4–6, we discovered that the data obtained using IR camera and what we computed using MRTI followed a similar trend. There are some reports in the literature that confirms such a similar trend [5,6,35,36].

The current study was aimed at looking more closely at the spatiotemporal heating generated during AuNP based photothermal therapy in a model made of agar gel to predict the response of cancer tissue to this therapy in the presence of AuNPs, which has already been demonstrated to be non-toxic and are already employed in clinical trials in humans [14,17,37–39]. To achieve this purpose, we used MRTI to produce thermometry. Since the heating depths cannot be predicted when a given laser exposure is employed, MRTI can possibly play an important role in the monitoring and control of nano-photothermal therapies in order to facilitate their translation into the clinic.

5. Conclusion

We employed MRTI to monitor temperature rise in the process of PTT. The PRF method as the most widely used MRTI technique can be considered in this process. Summarily, during the process of PTT, our MRTI studies confirmed:

(i) a significant temperature rise in AuNPs loaded phantoms,
(ii) a dependency between the rate of temperature rise and concentration of AuNPs,
(iii) a direct correlation between change of temperature and MR image phase.

We concluded that MRTI can be considered as a reasonable thermometry technique in the process of PTT because it had high correlation coefficient ($R > 0.9$) with an actual thermometer such as IR camera. Also, the recent research efforts have demonstrated the feasibility of incorporating MRTI to predict the profile of heat generation and distribution within an environment. Accordingly, it seems reasonable to develop a planning software system to facilitate the procedure of nanoparticle assisted PTT using MRTI, while simultaneously avoiding damage of critical organs. Such a planning software may present opportunities for patient selection and optimization of treatment approach.

Conflict of interest statement

The authors declare that they have no conflicts of interest.

Acknowledgement

This work was supported by Zahedan University of Medical Sciences (Grant number: 7970).

References

[1] J. Beik, Z. Abed, F.S. Ghoreishi, S. Hosseini-Nami, S. Mehrzadi, A. Shakeri-Zadeh, et al., Nanotechnology in hyperthermia cancer therapy: from fundamental principles to advanced applications, J. Control. Release 235 (2016) 205–221.
[2] J. Beik, S. Khademi, N. Attaran, S. Sarkar, A. Shakeri-Zadeh, H. Ghaznavi, et al., A nanotechnology based strategy to increase the efficiency of cancer diagnosis and therapy: folate conjugated gold nanoparticles, Curr. Med. Chem. 24 (2017) 4399–4416.
[3] N. Eyvazzadeh, A. Shakeri-Zadeh, R. Fekrazad, E. Amini, H. Ghaznavi, S.K. Kamrava, Gold-coated magnetic nanoparticle as a nanotheranostic agent for magnetic resonance imaging and photothermal therapy of cancer, Lasers Med. Sci. 32 (2017) 1469–1477.
[4] J. Beik, Z. Abed, A. Ghadimi-Daresajini, M. Nourbakhsh, A. Shakeri-Zadeh, M.S. Ghasemi, et al., Measurements of nanoparticle-enhanced heating from 1MHz ultrasound in solution and in mice bearing CT26 colon tumors, J. Therm. Biol. 62 (2016) 84–89.
[5] M.P. Melancon, A. Elliott, X. Ji, A. Shetty, Z. Yang, M. Tian, et al., Theranostics with multifunctional magnetic gold nanoshells: photothermal therapy and t2* magnetic resonance imaging, Invest. Radiol. 46 (2011) 132.
[6] R.J. Stafford, A. Shetty, A.M. Elliott, J.A. Schwartz, G.P. Goodrich, J.D. Hazle, MR temperature imaging of nanoshell mediated laser ablation, Int. J. Hyperth. 27 (2011) 782–790.
[7] A. Neshastehriz, M. Tabei, S. Maleki, S. Eynali, A. Shakeri-Zadeh, Photothermal therapy using folate conjugated gold nanoparticles enhances the effects of 6MV X-ray on mouth epidermal carcinoma cells, J. Photochem. Photobiol. B, Biol. 172 (2017) 52–60.
[8] X. Huang, P.K. Jain, I.H. El-Sayed, M.A. El-Sayed, Plasmonic photothermal therapy (PPTT) using gold nanoparticles, Lasers Med. Sci. 23 (2008) 217–228.
[9] H. Ghaznavi, S. Hosseini-Nami, S.K. Kamrava, R. Irajirad, S. Maleki, A. Shakeri-Zadeh, et al., Folic acid conjugated PEG coated gold–iron oxide core–shell nanocomplex as a potential agent for targeted photothermal therapy of cancer, Artif. Cells Nanomed. Biotechnol. 46 (8) (2018) 1594–1604.
[10] H. Samadian, S. Hosseini-Nami, S.K. Kamrava, H. Ghaznavi, A. Shakeri-Zadeh, Folate-conjugated gold nanoparticle as a new nanoplatform for targeted cancer therapy, J. Cancer Res. Clin. Oncol. 142 (2016) 2217–2229.
[11] A. Shakeri-Zadeh, S.K. Kamrava, M. Farhadi, Z. Hajikarimi, S. Maleki, A. Ahmadi, A scientific paradigm for targeted nanophotothermolysis; the potential for nanosurgery of cancer, Lasers Med. Sci. 29 (2014) 847–853.
[12] J. Huang, M. Guo, H. Ke, C. Zong, B. Ren, G. Liu, et al., Rational design and synthesis of γFe2O3@ Au magnetic gold nanoflowers for efficient cancer theranostics, Adv. Mater. 27 (2015) 5049–5056.
[13] V. Amendola, S. Scaramuzza, L. Litti, M. Meneghetti, G. Zuccolotto, A. Rosato, et al., Magneto-Plasmonic Au-Fe Alloy Nanoparticles Designed for Multimodal SERS-MRI-CT Imaging, Small. 10 (2014) 2476–2486.
[14] A. Kickhefel, J. Roland, C. Weiss, F. Schick, Accuracy of real-time MR temperature mapping in the brain: a comparison of fast sequences, Phys. Med. 26 (2010) 192–201.
[15] J. Olsrud, R. Wirestam, S. Brockstedt, A.M. Nilsson, K.-G. Tranberg, F. Ståhlberg, et al., MRI thermometry in phantoms by use of the proton resonance frequency shift method: application to interstitial laser thermotherapy, Phys. Med. Biol. 43 (1998) 2597.
[16] J. Hindman, Proton resonance shift of water in the gas and liquid states, J. Chem. Phys. 44 (1966) 4582–4592.
[17] W. James, L. Hirsch, J. West, P. O'Neal, J. Payne, Application of INAA to the build-up and clearance of gold nanoshells in clinical studies in mice, J. Radioanal. Nucl. Chem. 271 (2006) 455–459.
[18] A. Gaiduk, P.V. Ruijgrok, M. Yorulmaz, M. Orrit, Detection limits in photothermal microscopy, Chem. Sci. 1 (2010) 343–350.
[19] Y. Yue, J. Zhang, X. Wang, Micro/Nanoscale spatial resolution temperature probing for the interfacial thermal characterization of epitaxial graphene on 4H-SiC, Small 7 (2011) 3324–3333.
[20] Y. Gao, Y. Bando, Nanotechnology: carbon nanothermometer containing gallium, Nature 415 (2002) 599-.
[21] M.-H. Bae, Z.-Y. Ong, D. Estrada, E. Pop, Imaging, simulation, and electrostatic control of power dissipation in graphene devices, Nano Lett. 10 (2010) 4787–4793.
[22] A.R. Montazerabadi, M.A. Oghabian, R. Irajirad, S. Muhammadnejad, D. Ahmadvand, H.H. Delavari, et al., Development of gold-coated magnetic nanoparticles as a potential MRI contrast agent, NANO 10 (2015) 1550048.
[23] A. Curtis, M. Malekigorji, J. Holman, M. Skidmore, C. Hoskins, Heat dissipation of hybrid iron oxide-gold nanoparticles in an agar phantom, J. Nanomed. Nanotechnol. (2015) 6.
[24] A.M. Elliott, R.J. Stafford, J. Schwartz, J. Wang, A.M. Shetty, C. Bourgoyne, et al., Laser-induced thermal response and characterization of nanoparticles for cancer treatment using magnetic resonance thermal imaging, Med. Phys. 34 (2007) 3102–3108.
[25] F. Duck, Optical properties of tissue including ultraviolet and infrared radiation, Phys. Properties of Tissue. (1990) 43–71.
[26] P. Walker, R. Lerski, R. Mathur-De Vré, J. Binet, F. Yane VI, Preparation of agarose gels as reference substances for NMR relaxation time measurement, Magn. Reson. Imaging 6 (1988) 215–222.
[27] K.S. Brandenburg, A. Shakeri-Zadeh, G.A. Mansoori, Folate-conjugated gold nanoparticles for cancer nanotechnology applications, Proceedings of Nanotechnology

Conference (2011) 404–407.
[28] R. Vankayala, C.-C. Lin, P. Kalluru, C.-S. Chiang, K.C. Hwang, Gold nanoshells-mediated bimodal photodynamic and photothermal cancer treatment using ultra-low doses of near infra-red light, Biomaterials 35 (2014) 5527–5538.
[29] M. Aioub, S.R. Panikkanvalappil, M.A. El-Sayed, Platinum-coated gold nanorods: efficient reactive oxygen scavengers that prevent oxidative damage toward healthy, untreated cells during plasmonic photothermal therapy, ACS Nano 11 (2017) 579–586.
[30] D. Jaque, L.M. Maestro, B. Del Rosal, P. Haro-Gonzalez, A. Benayas, J. Plaza, et al., Nanoparticles for photothermal therapies, Nanoscale. 6 (2014) 9494–9530.
[31] Cancer nanotechnology treatment through folate conjugated gold, nanoparticles, in: A. Shakeri-Zadeh, G.A. Mansoori (Eds.), Proceedings of WCC (2010).
[32] J. Yin, D. Chen, S. Wu, C. Li, L. Liu, Y. Shao, Tumor-targeted nanoprobes for enhanced multimodal imaging and synergistic photothermal therapy: core–shell and dumbbell Gd-tailored gold nanorods, Nanoscale (2017).
[33] A. Majumdar, Scanning thermal microscopy, Annu. Rev. Mater. Sci. 29 (1999) 505–585.
[34] Y. Li, B.Q. Li, Use of CdTe quantum dots for high temperature thermal sensing, RSC Adv. 4 (2014) 24612–24618.
[35] Z. Chen, X. Shan, Y. Guan, S. Wang, J.-J. Zhu, N. Tao, Imaging local heating and thermal diffusion of nanomaterials with plasmonic thermal microscopy, ACS Nano 9 (2015) 11574–11581.
[36] D.A. Thayer, Y. Lin, A. Luk, G. Gulsen, Laser-induced photo-thermal magnetic imaging, Appl. Phys. Lett. 101 (2012) 083703.
[37] S. Khademi, S. Sarkar, S. Kharrazi, S.M. Amini, A. Shakeri-Zadeh, M.R. Ay, et al., Evaluation of size, morphology, concentration, and surface effect of gold nanoparticles on X-ray attenuation in computed tomography, Phys. Med. 45 (2018) 127–133.
[38] A. Shakeri-Zadeh, H. Eshghi, G. Mansoori, A. Hashemian, Gold nanoparticles conjugated with folic acid using mercaptohexanol as the linker, J. Nanotech. Prog. Int. (2009) 13–23.
[39] Y. Liu, X. Liu, X. Jin, P. He, X. Zheng, Z. Dai, et al., The dependence of radiation enhancement effect on the concentration of gold nanoparticles exposed to low-and high-LET radiations, Phys. Med. Eur. J. Med. Phys. 31 (2015) 210–218.